Stem Cell Reports
Report
ISSCR
OPEN ACCESS

PAX6-positive microglia evolve locally in hiPSC-derived ocular organoids

Nobuhiko Shiraki,[1] Kazuichi Maruyama,[1,2,3,*] Ryuhei Hayashi,[1,3,4] Akiko Oguchi,[5] Yasuhiro Murakawa,[5,6,7] Tomohiko Katayama,[1] Toru Takigawa,[1] Susumu Sakimoto,[1,3] Andrew J. Quantock,[8] Motokazu Tsujikawa,[9] and Kohji Nishida[1,3,*]

[1]Department of Ophthalmology, Osaka University Graduate School of Medicine, Osaka, Japan
[2]Department of Vision Informatics, Osaka University Graduate School of Medicine, Osaka, Japan
[3]Integrated Frontier Research for Medical Science Division, Institute for Open and Transdisciplinary Research Initiatives, Osaka University, Osaka, Japan
[4]Department of Stem Cells and Applied Medicine, Osaka University Graduate School of Medicine, Osaka, Japan
[5]RIKEN-IFOM Joint Laboratory for Cancer Genomics, RIKEN Center for Integrative Medical Sciences, Kanagawa, Japan
[6]Institute for the Advanced Study of Human Biology, Kyoto University, Kyoto, Japan
[7]Department of Medical Systems Genomics, Graduate School of Medicine, Kyoto University, Kyoto, Japan
[8]School of Optometry and Vision Sciences, Cardiff University, Cardiff, Wales, UK
[9]Department of Biomedical Informatics, Osaka University Graduate School of Medicine, Osaka, Japan
*Correspondence: kazuichi.maruyama@ophthal.med.osaka-u.ac.jp (K.M.), knishida@ophthal.med.osaka-u.ac.jp (K.N.)
https://doi.org/10.1016/j.stemcr.2021.12.009

SUMMARY

Microglia are the resident immune cells of the central nervous system (CNS). They govern the immunogenicity of the retina, which is considered to be part of the CNS; however, it is not known how microglia develop in the eye. Here, we studied human-induced pluripotent stem cells (hiPSCs) that had been expanded into a self-formed ectodermal autonomous multi-zone (SEAM) of cells that partially mimics human eye development. Our results indicated that microglia-like cells, which have characteristics of yolk-sac-like linage cells, naturally develop in 2D eye-like SEAM organoids, which lack any vascular components. These cells are unique in that they are paired box protein 6 (PAX6)-positive, yet they possess some characteristics of mesoderm. Collectively, the data support the notion of the existence of an isolated, locally developing immune system in the eye, which is independent of the body's vasculature and general immune system.

INTRODUCTION

The central nervous system (CNS) is inaccessible to immune cells in general circulation owing to the presence of the blood-brain barrier. Instead, microglial cells in the brain and spinal cord provide the CNS with its immune protection, acting against inflammation, degeneration, tumor growth, injury, trauma, and ischemic brain injury following cerebral infarction (Li and Barres, 2018; Tremblay et al., 2011). Microglia deliver immune protection for the posterior eye, including the neural retina, and have an involvement with some sight-threatening conditions, such as age-related macular degeneration, uveitis, glaucoma, and retinal degeneration (Rashid et al., 2019). Despite the key role of microglia in facilitating our immune defenses, their developmental origin has attracted controversy, and the question remains unresolved as to whether they emerge from the ectoderm or the mesoderm (Alekseeva et al., 2019; Ginhoux and Prinz, 2015). It is also uncertain whether or not microglia can form in isolation from the vasculature in tissues such as the eye.

Experiments on mouse embryos have indicated that adult microglia derive from primitive macrophage precursors that originate in the yolk sac before embryonic day 8, which thereafter proliferate (Ginhoux et al., 2010). A recent discovery by Muffat and associates has shown that microglia-like cells can be generated from human-induced pluripotent stem cells (hiPSCs) via myeloid differentiation (Muffat et al., 2016). Here, we show that PAX6-positive microglia-like cells, which we hereafter refer to as PAX6-positive microglia (PPM) cells, develop in hiPSC-derived eye-like self-formed ectodermal autonomous multi-zone (SEAM) organoids (Hayashi et al., 2016). This points to the existence of a local immune system in the eye that is isolated from the general immune system. Our novel findings did not investigate the development of microglia precisely since the SEAM is a 2D model and not a 3D model. However, given that the SEAM lacks vascular components, our data suggest that human microglia may develop in the absence of a blood supply.

RESULTS

Microglia-like cells evolve in hiPSC-derived SEAMs

Typical four-zoned eye-like SEAM organoids (Figure 1A) were generated from 201B7 hiPSCs and subjected to immunostaining for markers of immune cells. This revealed that retinal and retinal pigment epithelium cells in SEAM 2, along with ocular surface cells in SEAM 3, were positive for *CD11b*, transmembrane protein 119 (TMEM119), and CX3C chemokine receptor 1 (CX3CR1) (Figures 1B–1E; Videos S1a and S1b). Previous reports have disclosed that CNS macrophages and microglia express CD11b and CX3CR1 and that microglia are positive for TMEM119 (Bennett et al., 2016; Ford et al., 1995; Martin et al., 2017). This supports the contention

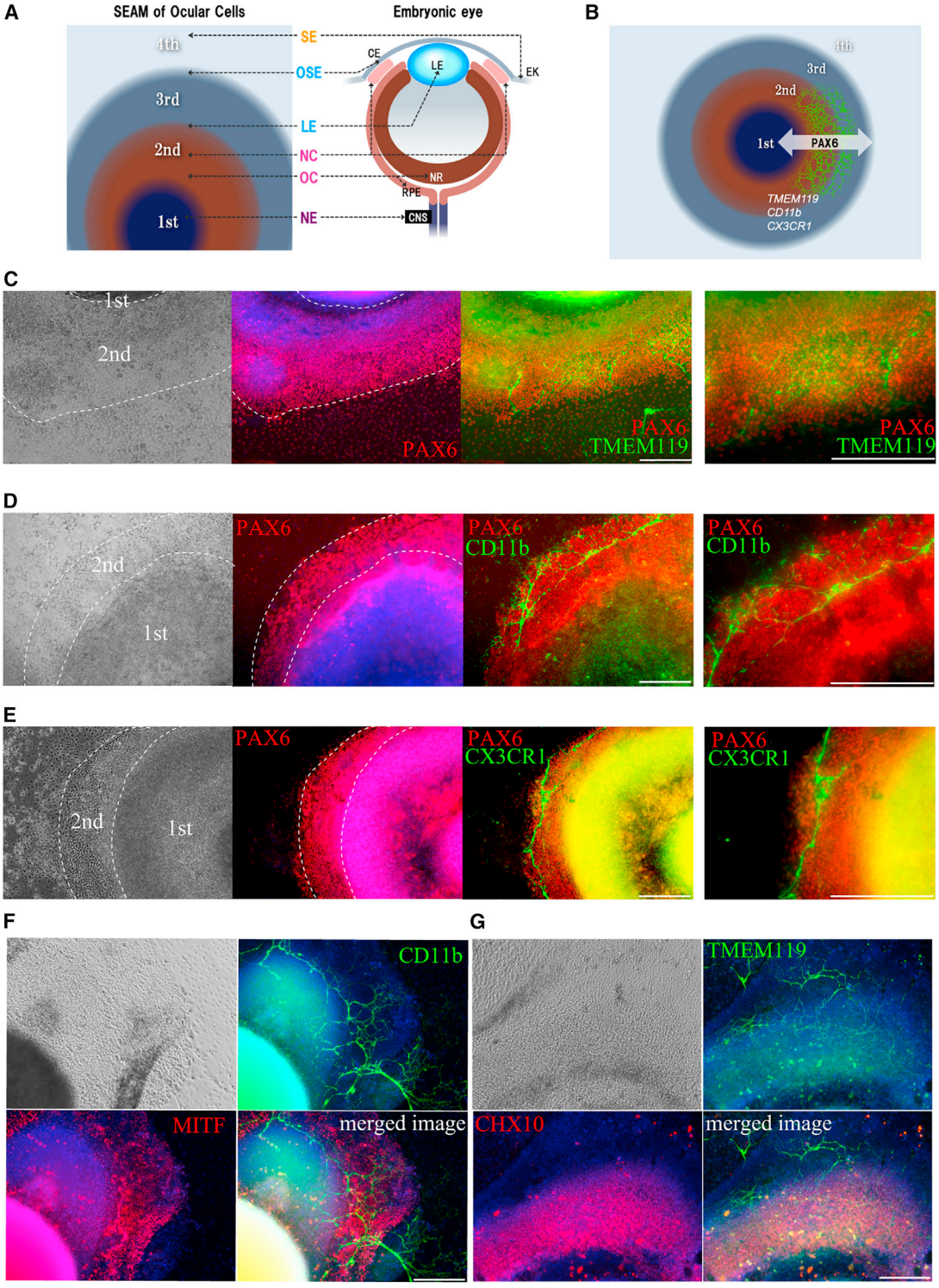

Figure 1. Spontaneously generated PPM cells in a 2D SEAM of human eye development

(A) A self-formed ectodermal autonomous multi-zone (SEAM) derived from hiPSCs contains cells of ectodermal lineage that mimic anterior and posterior eye development *in vivo*. CNS, central nervous system; NE, neuroectoderm; OC, optic cup; NR, neuroretina; NC, neural crest; LE; lens; OSE, ocular surface ectoderm; SE, surface ectoderm; CE, corneal epithelium; EK, epidermal keratinocyte.

(B) Schematic showing the expression pattern of microglia-related genes in the SEAM.

(legend continued on next page)

that microglia-like cells evolve in hiPSC-derived eye-like SEAMs. Perivascular macrophages and the microglia marker CD68 were not detected in the SEAM (Figure S1A) (Fiala et al., 2002) nor were the Muller and astrocyte markers glial fibrillary acidic protein (GFAP), RLBP1, and CHX10 (Figures S1B–S1D) at 4 weeks (Suga et al., 2014). CD11b- and TMEM119-positive cells were not detected at day 8 of SEAM development (Figures S1E and S1F) but became evident from day 10 onwards (Figures S1G and S1H), forming a circumferential network at the border of SEAMs 2 and 3. By day 14, circumferential and radial patternings of cells that stained positive for these microglial markers were apparent (Figures S1I and S1J) and persisted when the cultivation media was switched to one that supported SEAM differentiation into retina-like tissue (Figures 1F, 1G, and S1K). Similar results were found when another hiPSC line (D2) was studied and when human embryonic stem cells (KhES-1) were investigated (Figures 2A–2D). Quantitative reverse-transcription polymerase chain reaction (qRT-PCR) of the SEAM at days 14, 21, and 28 revealed the expression of a number of immune cells markers (Figures 2E and S2A). Together, the immunolabelling and qRT-PCR findings indicated that microglial-like cells emerge in SEAMs. qRT-PCR of the SEAM at day 7 of cultivation, used to probe early development, confirmed the expression of *PAX6*, an early developmental marker of the neuroectoderm and ocular cells (Figure 3A) (Chow et al., 1999; Zhang et al., 2010). Endoderm markers *GATA4* and *SOX17*, mesoderm markers *NKX2-5*, *SNAL1*, and *TBX3*, meso-endoderm marker *T*, and *PU.1* (an essential factor required for the development of the yolk sac and myeloid system [Kierdorf et al., 2013]) were not detected (Figure 3A). It was also found that almost all cells were stained PAX6 or p63, a surface ectodermal marker (Yoh and Prywes, 2015), at the 4-week culture point just before cell sorting (Figures S2B–S2F).

Gene expression, cytokine stimulation, and phagocytosis

To further interrogate PPM cells, they were isolated from 28-day-expanded SEAMs using fluorescence-activated cell sorting (FACS) according to the expression of a combination of CD11b and CD45. CD11b-positive cells include microglia and CNS macrophages, with CD45 labeling used to distinguished PPM cells from macrophages based on the high levels of CD45 expression in macrophages compared with microglia (Ford et al., 1995). This analysis revealed that 0.33% ± 0.12% of cells (n = 8) were CD11b-positive PPM cells (Figure 3B). After PPM cells were cultured for just 24 h for cell recovery, to probe cell function, these were stimulated alongside immortalized human microglia cells (abm, Richmond, QC, Canada) with lipopolysaccharide (LPS), interferon gamma (IFN-γ), and transforming growth factors β1 and β2 (TGF-β1 and -β2) (Figure S3A). RNA sequencing revealed that the expression levels of several genes associated with primary microglia were higher in PPM cells than in immortalized human microglial cells (Figure 3C) (Ayata et al., 2018; Galatro et al., 2017; Gautier et al., 2012; Gosselin et al., 2017; Hickman et al., 2013). *PAX6* expression levels, along with those of microglial cell immune genes, were elevated in PPM cells (Figures 3D and 3E). The expression levels of microglia-associated genes in PPM cells also fluctuated with the stimulation conditions, which has potential functional relevance. Cytokine levels in the culture medium after the stimulation of PPM cells revealed the expression of interleukin (IL)-6 and IL-8, but not IL-1β, IL-4, IL-10, or tumor necrosis factor (TNF)-α (Figures 3F and S3B). IL-8 expression was significantly higher in the immortalized human microglia group than in the PPM group ($p < 0.0001$), whereas the opposite was true for IL-6, with higher expression levels in PPM cells ($p < 0.0001$). IL-6 levels were significantly higher in LPS- and IFN-γ-stimulated conditions for both PPM and immortalized microglial groups when compared with non-stimulated and LPS-only stimulated conditions ($p = 0.003$, $p = 0.02$). The amount of IL-8 secreted from PPM cells was less than that from immortalized human microglia cells. Expression levels of vascular epithelial growth factor A (*VEGFA*), which increases when microglia are stimulated (Ding et al., 2018), did not change following cytokine stimulation in immortalized human microglial cells but did increase when the PPM cells were stimulated. *VEGFA* expression in PPM cells was significantly higher after TGF-β1 stimulation compared with no cytokine stimulation ($p = 0.04$). *TGF-β2* expression, moreover, was significantly higher in PPM cells than in immortalized human microglia cells ($p < 0.0001$) (Figure 3G). TGF-β2 secretion of the TGF-β2 stimulated PPM cells was significantly higher than that found for combined LPS- and IFN-γ stimulation ($p = 0.0062$). A phagocytosis test of PPM cells revealed that the PPM cells did not phagocytose the microspheres (Figure S3C).

(C–E) Immunostaining of PAX6 (red) in zones 1–3 of a 4-week, cultivated 201B7 hiPSC-derived SEAM along with staining of nuclei (blue) and TMEM119 (C, green), CD11b (D, green), and CX3CR1 (E, green).

(F and G) Immunostaining after 7 weeks of differentiation for retinal culture: (F) CD11b (green) and MITF retinal pigment epithelium cells (red) and (G) TMEM119 (green) and CHX10 neuro-retinal cells (red). Images are representative of three independent experiments. Scale bar, 200 μm.

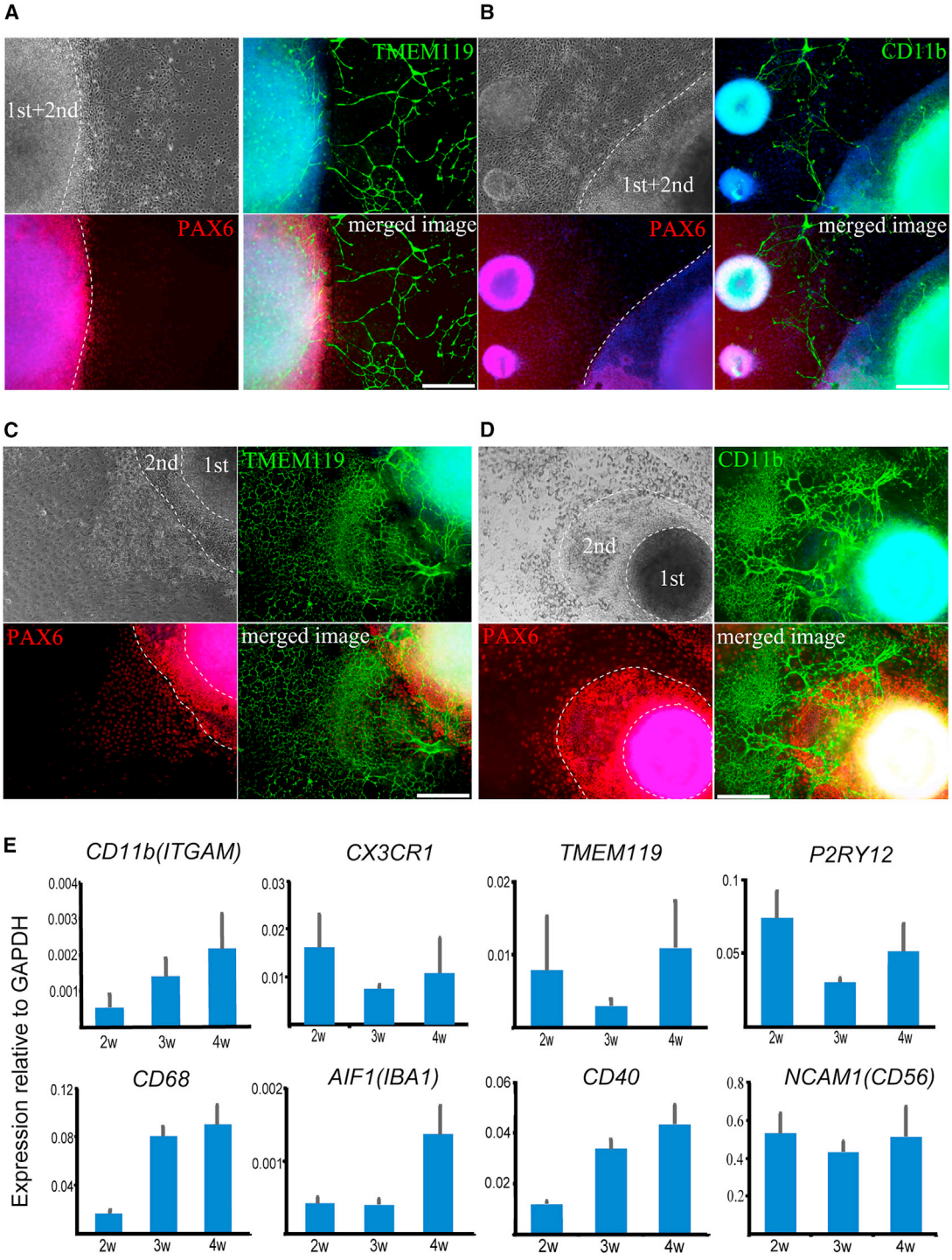

Figure 2. Immunostaining of differently derived SEAMs and expression of immune cell markers

(A and B) hES KhES-1-derived SEAMs after 4 weeks of culture immunostained with (A) TMEM119 (green) and PAX6 (red) and (B) CD11b (green) and PAX6 (red).

(C and D) 1383D2 hiPSC-derived SEAMs after 4 weeks of culture immunostained with (C) TMEM119 (green) and PAX6 (red) and (D) CD11b (green) and PAX6 (red). Images are representative of multiple independent experiments. Nuclei are in blue. Scale bar, 200 μm.

(E) Gene expression analysis of immune-related markers in SEAMs after 4 weeks of culture (six independent experiments). Error bars show standard deviation (SD).

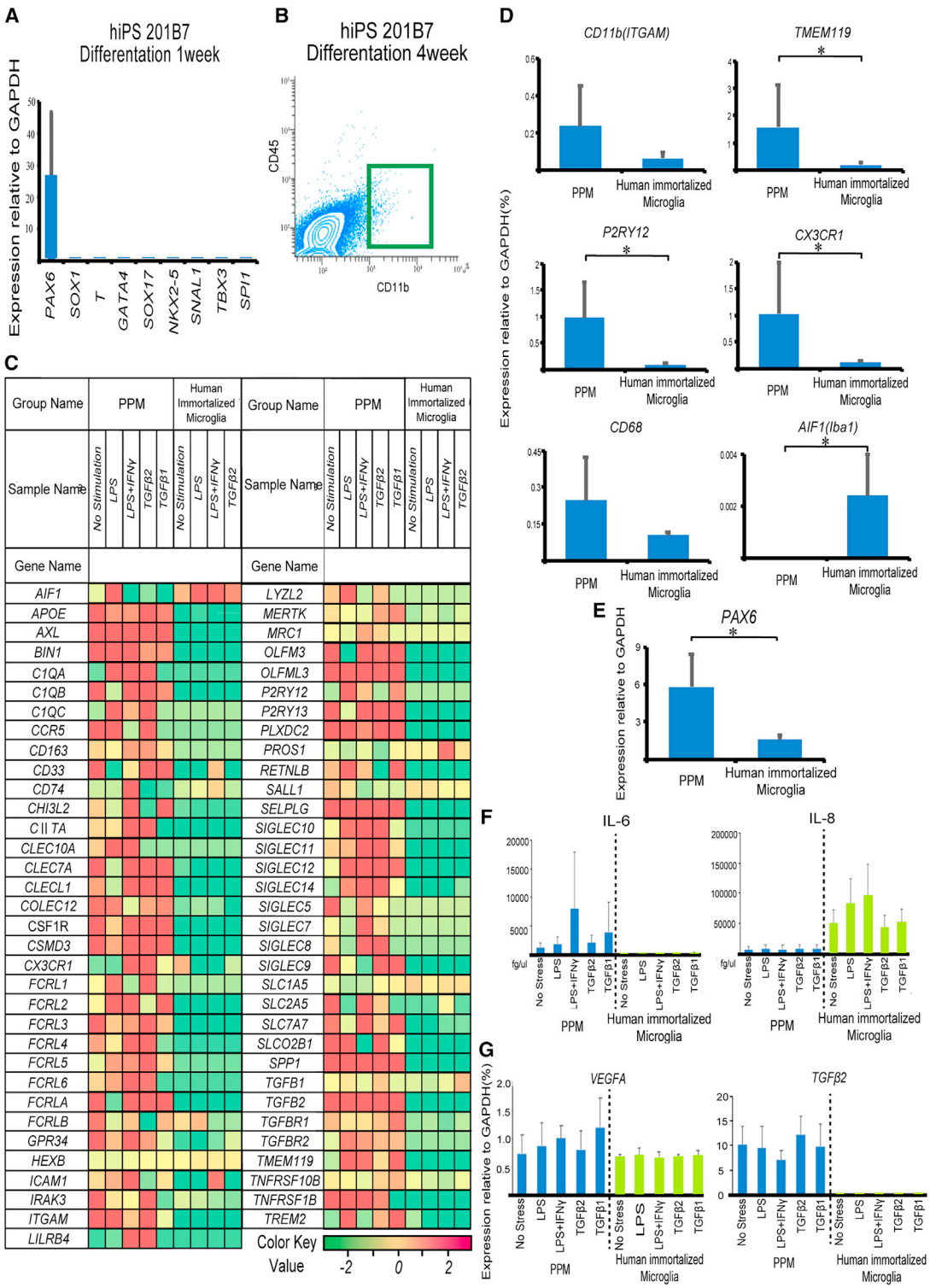

Figure 3. Developmental and immune cell markers in a SEAM, and isolation and analysis of PPM cells

(A) Gene expression analysis of development-related markers in a SEAM after 1 week of culture (six independent experiments).

(B) Flow cytometric analysis of CD11b and CD45 in differentiated hiPSCs after 27–28 days of culture, with PPM cells indicated (box). Data are representative of seven independent cell-sorting experiments.

(C) RNA-seq data of PPM cells and human immortalized microglia. Both cell types were stimulated for 24 h.

(legend continued on next page)

Single-cell RNA sequencing

Despite the fact that there was some heterogeneity in the data, which was likely caused by cellular immaturity or limitations of sorting, single-cell RNA sequencing showed that, overall, PPM cells are more similar to yolk-sac-derived, myeloid-based progenitors (YSMP) cells than other human embryonic hematopoietic cells, such as microglia and macrophages (Figures 4A, 4B, S4A, and S4B; Table S1) (Bian et al., 2020). Zhilei Bian et al. reported human tissue-resident macrophage, microglia, YSMPs, and other immune cells from a human embryo at Carnegie stages 11–23. We compared our single-cell RNA sequencing data of PPM cells with the human embryo immune cell data they reported, as detailed in the Supplemental experimental procedures. They defined a yolk-sac-derived progenitor population, which appeared in the yolk sac at CS11, showed much weaker transcriptomic erythroid features than mouse erythromyeloid progenitors, and had a myeloid-biased nature, as YSMP. In particular, PPM cells expressed the PAX6 and YSMP markers (Figures 4C–4E). The PPM cells were divided into several clusters, which was thought to be due to immaturity of the cells. Cumulatively, the data point to a unique type of immune cell, referred to here as a PPM cell, that evolves in the eye (and in the retina especially) locally and in isolation from the general immune system.

DISCUSSION

In this study, we provided the possibility that ocular microglia-like cells emerge naturally and locally in the eye and are PAX6-positive. The origin of ocular microglia, the predominant innate immune cell system in the sensory retina as part of the CNS, has been the subject of considerable debate for decades. The conventional theory holds that microglia develop in the yolk sac and travel to the brain (possibly including the retina, a part of the CNS) through the bloodstream during early development before the closure of the blood-brain barrier (Alliot et al., 1999). Arguing against this notion, however, is the fact that microglia are present in the avascular retina of birds (Navascues et al., 1994) and that they appear in human and mouse retinas prior to vascularization (Diaz-Araya et al., 1995; Santos et al., 2008). Here, we used a previously described technology (Hayashi et al., 2016), in which hiPSCs form 2D SEAM eye-like organoids, and show that SEAMs include PPM cells, which emerge spontaneously under simple and natural differentiation conditions in the absence of any factors that mimic blood circulation. Thus, PPM cells that develop in hiPSC-derived SEAM organoids do so in the absence of a vasculature.

Stimulation of PPM cells by LPS did not elicit any cytokine response, and in this regard, they are unlike normal microglia (Lund et al., 2006). LPS stimulation increases IL-6 expression in microglia generated from both primary mouse microglia and from hiPSCs via the mesoderm, leading us to conclude that PPM cells are distinct from bone-marrow-derived or mesoderm-derived microglia. The present investigation also reveals that PPM cells and immortalized human microglia cells differ in their responses to inflammation stimulation. The eye is said to have partial immune privilege, and the introduction of LPS into the vitreous cavity does not induce ocular inflammation (Stein-Streilein, 2013). This is consistent with the finding that PPM cells, as the sole immune gatekeepers of the eye's posterior segment, do not respond to LPS stimuli.

Direct regulation of autoreactive regulatory T cells is the major mechanism by which TGF-β maintains tolerance (Gorelik and Flavell, 2000). TGF-β2 is the chief immune-modulating factor in the aqueous humor of the eye (a fluid similar to plasma) and acts to generate tolerogenic antigen-presenting cells. Bone marrow cells, on the other hand, can be activated to produce TGF-β1 (Cousins et al., 1991; Stein-Streilein, 2013). TGF-β2 plays a pivotal role in the immune system in maintaining tolerance, primarily by regulating lymphocyte proliferation, differentiation, and survival (Stein-Streilein, 2013). *TGFB2* expression in PPM cells is elevated after TGF-β2 exposure, whereas IL-6, IL-8, and *VEGFA* levels remain unchanged. Exposure to TGF-β1, which is constantly maintained at low levels in the eye, stimulated inflammation and upregulated the expression level of *VEGFA* in PPM cells. Similarly, exposure to IFN-γ (which is present at low levels in the eye) resulted in inflammatory stimulation, with a high expression of IL-6 and a low expression of TGF-β2 and IL-8. This suggests that IFN-γ-stimulated microglia may induce $Foxp3^{+}$ $CD8^{+}$ regulatory T cells in ocular tissue (Nakagawa et al., 2010). Based on these results, we conclude that PPM cells may perform similar functions as M2-type-activated microglia, and that this may impact upon immune tolerance and suppression in ocular tissue. Similar tendencies were observed in immortalized human microglia, although with lower expression levels of *TGF-β2* than

(D and E) Gene expression analysis of (D) microglia-related markers and (E) *PAX6* in PPM cells and human immortalized microglia cells (data from four independent experiments). *$p < 0.05$ by the Mann-Whitney rank-sum test.
(F) IL-6 and IL-8 levels after stimulation of PPM cells in 10–16 independent experiments.
(G) Gene expression analysis of *VEGFA* and *TGFB2* after stimulating PPM cells (data from seven to ten independent experiments). Error bars show SD.

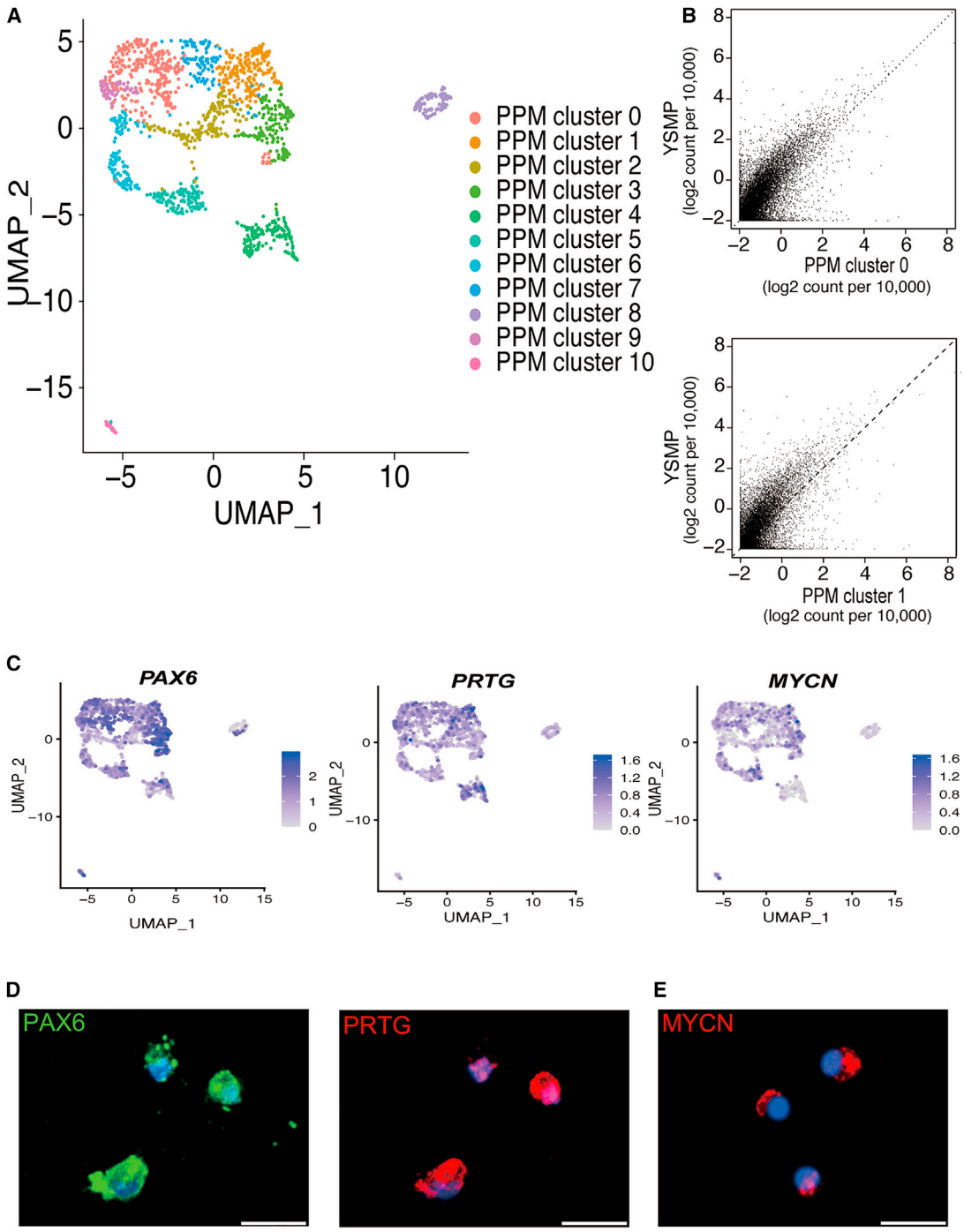

Figure 4. Single-cell RNA-seq analysis of CD11b + cells in a SEAM

(A) Uniform manifold approximation and projection (UMAP) plot visualizing 1,498 CD11b + cells and colored based on 11 cluster types.

(B) Scatterplot showing the gene expression of PPM cluster_0 and 1 identified in CD11b + scRNA-seq and of a YSMP cluster in scRNA-seq of embryonic macrophages.

(C) Feature plots of *PAX6*, *PTRG*, and *MYCN* expression. The expression levels of each cell type are colored in the UMAP plot.

(D and E) Immunostaining of (D) PAX6 (green) and PRTG (red) and (E) MYCN (red). CD11b + cells were sorted by FACS and cytospin after 4 weeks of culture. Images represent three independent experiments. Nuclei are in blue. Scale bar, 25 μm.

are found in PPM cells. PPM cells are limited in phagocytosis tests and some functions, which could be attributed to immaturity or other causes. Further attempts at maturation and examination of their functions may contribute to a better understanding of the immune system of the eye. Additionally, this model is a 2D model, and a 3D model of the entire eye (including cornea, conjunctiva, neural retina, retinal pigment epithelium [RPE], lens, etc.) is yet to be created; however, a 3D model of the neural retina (Eiraku et al., 2011; Zhong et al., 2014) has been created. The development of a 3D model of human ocular development will enable us to study the immune system more thoroughly.

A gene expression analysis revealed that PPM cells have unique properties. For example, they express microglia-specific genes, such as *CD11b*, *TMEM119*, and *CX3CR1*. Single-cell gene expression investigations further point to similarities to YSMP cells, with the microglial population positive for PAX6 (this was supported by immunostaining of isolated microglial cells with cytospin). *PAX6* is considered to be an ocular master control gene (Chow et al., 1999; Halder et al., 1995) and is necessary for eye development in flies to humans (Hill et al., 1991; Nakayama et al., 2015). It is required for the differentiation of most retinal lineages, and when PAX6 is inactivated in retinal progenitor cells, they do not form retinal cells (Marquardt et al., 2001). PAX6 is also highly expressed in the anterior segment structures of the eye that are derived from surface ectoderm, such as the lens vesicle and corneal and conjunctival epithelia (Shaham et al., 2012; Terzic and Saraga-Babic, 1999). *PAX6*, moreover, is necessary and sufficient for the differentiation of human embryonic stem cells (ESCs) to neuroectoderm, and while it is dispensable for mouse ESC development, it is a generic neuroectodermal specification factor in primates (Zhang et al., 2010). Thus, PPM cells that emerge in hiPSC-derived SEAMs likely have a neuroectodermal origin but also possess some features of mesodermal cells. This suggests that some retinal microglia are neuroectodermally derived cells, which retain some properties of the mesoderm. This notion is complementary to, rather than contrary to, previous reports, which show that some retinal microglia are likely to be neuroectodermally derived cells with mesodermal properties (Ginhoux et al., 2010) and that microglia that repopulate the adult mouse brain after experimental depletion do so via the proliferation of cells that are positive for an ectodermal neural stem cell marker (Elmore et al., 2014). The findings significantly enhance our understanding of the origin of microglia that regulate the immune system of the CNS, especially the retina, and raise the possibility of locally developing immune systems involving cells such as resident macrophages in the brain or other organs.

EXPERIMENTAL PROCEDURES

Detailed methods are provided in the Supplemental experimental procedures.

Flow cytometry and cell sorting

SEAMs cultured in DM for 4 weeks were dissociated using Accumax (Life Technologies) for 10 min at 37°C and resuspended in an ice-cold cell-staining buffer (420201, BioLegend, San Diego, CA, USA), after which the harvested cells were filtered using a cell strainer. They were stained with a CD11b-fluorescein isothiocyanate (FITC) antibody (101206, BioLegend); FITC rat IgG2b (400605, BioLegend); phycoerythrin (PE)/cyanine7 anti-human CD45 (304016, BioLegend); PE/Cy7 mouse IgG1 (400126, BioLegend); an APC anti-human CD45 antibody (304,037, BioLegend); and APC mouse IgG1 (400120, BioLegend) for 30 min on ice (Ford et al., 1995; Sedgwick et al., 1991). After washing three times with PBS, the stained cells were sorted using a FACSAria II instrument (BD Biosciences), and the data were analyzed using BD FACSDiva software (BD Biosciences). CD11b-positive cells, which did not express high levels of CD45, were harvested. After sorting, some of the cells were used for cytospin, while the remaining cells (now with the identity of PPM cells) were seeded on poly-D-lysine-coated (1.3 g/cm^2) and LN511E8-coated (0.5 μg/cm^2) dishes at the density of 1.6–2.4 × 10^5 cells/cm^2 and cultured in microglial culture medium (MCM; DMEM/F12 [1:1] supplemented with 10% FBS [Japan Bio Serum, Hiroshima, Japan], 1% GultaMAX [Thermo Fisher Scientific], and 1% penicillin-streptomycin solution). The sorted PPM cells were adjusted to a density of 2 × 10^5 cells/mL, after which 200 μL of the cell suspension was centrifuged at 1,000 RPM for 5 min in a Cytospin 4 Cytocentrifuge (Thermo Fisher Scientific).

Cell stimulation

To examine the effect of inflammatory agents, PPM cells and immortalized microglia cells were cultured for 24 h and further stimulated for 24 h with LPS (1 μg/mL) (Sigma-Aldrich), LPS (1 μg/mL) and IFN-γ (200 ng/mL) (Wako), TGF-β2 (5 ng/mL) (R&D Systems, Minneapolis, MN, USA), or TGF-β1 (5 ng/mL) (Wako) added to the culture media. The medium was then collected in protein low-adhesion tubes, and the cells were stored in QIAzol reagent (Qiagen, Valencia, CA, USA).

Resource availability

Details are provided in the Supplemental resource availability.

SUPPLEMENTAL INFORMATION

Supplemental information can be found online at https://doi.org/10.1016/j.stemcr.2021.12.009.

AUTHOR CONTRIBUTIONS

N.S. and K.M. designed the study; N.S. designed and performed the experiments and analyzed the data; T.K. performed hESC differentiation and analyzed the data; T.T., S.S., A.O., and Y.M. assisted in analyzing single-cell RNA sequencing (RNA-seq) data; N.S., K.M., A.J.Q., and K.N. analyzed the data and wrote the manuscript;

R.H., M.T., and K.N. provided conceptual advice regarding the study design.

CONFLICT OF INTERESTS

The authors declare no competing interests.

ACKNOWLEDGMENTS

We thank Y. Ishikawa, Y. Kobayashi, S. Shibata, S. Inoue, Y. Yasukawa, and M. Morita of Osaka University for technical assistance. We acknowledge the NGS core facility of the Genome Information Research Center at the Research Institute for Microbial Diseases of Osaka University for assistance in RNA sequencing and data analysis. This research was supported by AMED under grant number 20gm1210004, by JSPS KAKENHI under grant number JP17K11475, and by the Integrated Frontier Research for Medical Science Division, Institute for Open and Transdisciplinary Research Initiatives, Osaka University.

Received: September 15, 2021
Revised: December 13, 2021
Accepted: December 14, 2021
Published: January 13, 2022

REFERENCES

Alekseeva, O.S., Kirik, O.V., Gilerovich, E.G., and Korzhevskii, D.E. (2019). Microglia of the brain: origin, structure, functions. J. Evol. Biochem. Physiol. *55*, 257–268. https://doi.org/10.1134/s002209301904001x.

Alliot, F., Godin, I., and Pessac, B. (1999). Microglia derive from progenitors, originating from the yolk sac, and which proliferate in the brain. Brain Res. Dev. Brain Res. *117*, 145–152. https://doi.org/10.1016/s0165-3806(99)00113-3.

Ayata, P., Badimon, A., Strasburger, H.J., Duff, M.K., Montgomery, S.E., Loh, Y.E., Ebert, A., Pimenova, A.A., Ramirez, B.R., Chan, A.T., et al. (2018). Epigenetic regulation of brain region-specific microglia clearance activity. Nat. Neurosci. *21*, 1049–1060. https://doi.org/10.1038/s41593-018-0192-3.

Bennett, M.L., Bennett, F.C., Liddelow, S.A., Ajami, B., Zamanian, J.L., Fernhoff, N.B., Mulinyawe, S.B., Bohlen, C.J., Adil, A., Tucker, A., et al. (2016). New tools for studying microglia in the mouse and human CNS. Proc. Natl. Acad. Sci. U S A *113*, E1738–E1746. https://doi.org/10.1073/pnas.1525528113.

Bian, Z., Gong, Y., Huang, T., Lee, C.Z.W., Bian, L., Bai, Z., Shi, H., Zeng, Y., Liu, C., He, J., et al. (2020). Deciphering human macrophage development at single-cell resolution. Nature *582*, 571–576. https://doi.org/10.1038/s41586-020-2316-7.

Chow, R.L., Altmann, C.R., Lang, R.A., and Hemmati-Brivanlou, A. (1999). Pax6 induces ectopic eyes in a vertebrate. Development *126*, 4213–4222.

Cousins, S.W., McCabe, M.M., Danielpour, D., and Streilein, J.W. (1991). Identification of transforming growth factor-beta as an immunosuppressive factor in aqueous humor. Invest. Ophthalmol. Vis. Sci. *32*, 2201–2211.

Diaz-Araya, C.M., Provis, J.M., Penfold, P.L., and Billson, F.A. (1995). Development of microglial topography in human retina. J. Comp. Neurol. *363*, 53–68. https://doi.org/10.1002/cne.903630106.

Ding, X., Gu, R., Zhang, M., Ren, H., Shu, Q., Xu, G., and Wu, H. (2018). Microglia enhanced the angiogenesis, migration and proliferation of co-cultured RMECs. BMC Ophthalmol. *18*, 249. https://doi.org/10.1186/s12886-018-0886-z.

Eiraku, M., Takata, N., Ishibashi, H., Kawada, M., Sakakura, E., Okuda, S., Sekiguchi, K., Adachi, T., and Sasai, Y. (2011). Self-organizing optic-cup morphogenesis in three-dimensional culture. Nature *472*, 51–56. https://doi.org/10.1038/nature09941.

Elmore, M.R., Najafi, A.R., Koike, M.A., Dagher, N.N., Spangenberg, E.E., Rice, R.A., Kitazawa, M., Matusow, B., Nguyen, H., West, B.L., and Green, K.N. (2014). Colony-stimulating factor 1 receptor signaling is necessary for microglia viability, unmasking a microglia progenitor cell in the adult brain. Neuron *82*, 380–397. https://doi.org/10.1016/j.neuron.2014.02.040.

Fiala, M., Liu, Q.N., Sayre, J., Pop, V., Brahmandam, V., Graves, M.C., and Vinters, H.V. (2002). Cyclooxygenase-2-positive macrophages infiltrate the Alzheimer's disease brain and damage the blood-brain barrier. Eur. J. Clin. Invest. *32*, 360–371. https://doi.org/10.1046/j.1365-2362.2002.00994.x.

Ford, A.L., Goodsall, A.L., Hickey, W.F., and Sedgwick, J.D. (1995). Normal adult ramified microglia separated from other central nervous system macrophages by flow cytometric sorting. Phenotypic differences defined and direct ex vivo antigen presentation to myelin basic protein-reactive CD4+ T cells compared. J. Immunol. *154*, 4309–4321.

Galatro, T.F., Holtman, I.R., Lerario, A.M., Vainchtein, I.D., Brouwer, N., Sola, P.R., Veras, M.M., Pereira, T.F., Leite, R.E.P., Moller, T., et al. (2017). Transcriptomic analysis of purified human cortical microglia reveals age-associated changes. Nat. Neurosci. *20*, 1162–1171. https://doi.org/10.1038/nn.4597.

Gautier, E.L., Shay, T., Miller, J., Greter, M., Jakubzick, C., Ivanov, S., Helft, J., Chow, A., Elpek, K.G., Gordonov, S., et al. (2012). Gene-expression profiles and transcriptional regulatory pathways that underlie the identity and diversity of mouse tissue macrophages. Nat. Immunol. *13*, 1118–1128. https://doi.org/10.1038/ni.2419.

Ginhoux, F., Greter, M., Leboeuf, M., Nandi, S., See, P., Gokhan, S., Mehler, M.F., Conway, S.J., Ng, L.G., Stanley, E.R., et al. (2010). Fate mapping analysis reveals that adult microglia derive from primitive macrophages. Science *330*, 841–845. https://doi.org/10.1126/science.1194637.

Ginhoux, F., and Prinz, M. (2015). Origin of microglia: current concepts and past controversies. Cold Spring Harb. Perspect. Biol. *7*, a020537. https://doi.org/10.1101/cshperspect.a020537.

Gorelik, L., and Flavell, R.A. (2000). Abrogation of TGFbeta signaling in T cells leads to spontaneous T cell differentiation and autoimmune disease. Immunity *12*, 171–181. https://doi.org/10.1016/s1074-7613(00)80170-3.

Gosselin, D., Skola, D., Coufal, N.G., Holtman, I.R., Schlachetzki, J.C.M., Sajti, E., Jaeger, B.N., O'Connor, C., Fitzpatrick, C., Pasillas, M.P., et al. (2017). An environment-dependent transcriptional

network specifies human microglia identity. Science *356*. https://doi.org/10.1126/science.aal3222.

Halder, G., Callaerts, P., and Gehring, W.J. (1995). Induction of ectopic eyes by targeted expression of the eyeless gene in Drosophila. Science *267*, 1788–1792. https://doi.org/10.1126/science.7892602.

Hayashi, R., Ishikawa, Y., Sasamoto, Y., Katori, R., Nomura, N., Ichikawa, T., Araki, S., Soma, T., Kawasaki, S., Sekiguchi, K., et al. (2016). Co-ordinated ocular development from human iPS cells and recovery of corneal function. Nature *531*, 376–380. https://doi.org/10.1038/nature17000.

Hickman, S.E., Kingery, N.D., Ohsumi, T.K., Borowsky, M.L., Wang, L.C., Means, T.K., and El Khoury, J. (2013). The microglial sensome revealed by direct RNA sequencing. Nat. Neurosci. *16*, 1896–1905. https://doi.org/10.1038/nn.3554.

Hill, R.E., Favor, J., Hogan, B.L., Ton, C.C., Saunders, G.F., Hanson, I.M., Prosser, J., Jordan, T., Hastie, N.D., and van Heyningen, V. (1991). Mouse small eye results from mutations in a paired-like homeobox-containing gene. Nature *354*, 522–525. https://doi.org/10.1038/354522a0.

Kierdorf, K., Erny, D., Goldmann, T., Sander, V., Schulz, C., Perdiguero, E.G., Wieghofer, P., Heinrich, A., Riemke, P., Holscher, C., et al. (2013). Microglia emerge from erythromyeloid precursors via Pu.1- and Irf8-dependent pathways. Nat. Neurosci. *16*, 273–280. https://doi.org/10.1038/nn.3318.

Li, Q., and Barres, B.A. (2018). Microglia and macrophages in brain homeostasis and disease. Nat. Rev. Immunol. *18*, 225–242. https://doi.org/10.1038/nri.2017.125.

Lund, S., Christensen, K.V., Hedtjarn, M., Mortensen, A.L., Hagberg, H., Falsig, J., Hasseldam, H., Schrattenholz, A., Porzgen, P., and Leist, M. (2006). The dynamics of the LPS triggered inflammatory response of murine microglia under different culture and in vivo conditions. J. Neuroimmunol. *180*, 71–87. https://doi.org/10.1016/j.jneuroim.2006.07.007.

Marquardt, T., Ashery-Padan, R., Andrejewski, N., Scardigli, R., Guillemot, F., and Gruss, P. (2001). Pax6 is required for the multipotent state of retinal progenitor cells. Cell *105*, 43–55. https://doi.org/10.1016/s0092-8674(01)00295-1.

Martin, E., El-Behi, M., Fontaine, B., and Delarasse, C. (2017). Analysis of microglia and monocyte-derived macrophages from the central nervous system by flow cytometry. J. Vis. Exp. https://doi.org/10.3791/55781.

Muffat, J., Li, Y., Yuan, B., Mitalipova, M., Omer, A., Corcoran, S., Bakiasi, G., Tsai, L.H., Aubourg, P., Ransohoff, R.M., and Jaenisch, R. (2016). Efficient derivation of microglia-like cells from human pluripotent stem cells. Nat. Med. *22*, 1358–1367. https://doi.org/10.1038/nm.4189.

Nakagawa, T., Tsuruoka, M., Ogura, H., Okuyama, Y., Arima, Y., Hirano, T., and Murakami, M. (2010). IL-6 positively regulates Foxp3+CD8+ T cells in vivo. Int. Immunol. *22*, 129–139. https://doi.org/10.1093/intimm/dxp119.

Nakayama, T., Fisher, M., Nakajima, K., Odeleye, A.O., Zimmerman, K.B., Fish, M.B., Yaoita, Y., Chojnowski, J.L., Lauderdale, J.D., Netland, P.A., and Grainger, R.M. (2015). Xenopus pax6 mutants affect eye development and other organ systems, and have phenotypic similarities to human aniridia patients. Dev. Biol. *408*, 328–344. https://doi.org/10.1016/j.ydbio.2015.02.012.

Navascues, J., Moujahid, A., Quesada, A., and Cuadros, M.A. (1994). Microglia in the avian retina: immunocytochemical demonstration in the adult quail. J. Comp. Neurol. *350*, 171–186. https://doi.org/10.1002/cne.903500203.

Rashid, K., Akhtar-Schaefer, I., and Langmann, T. (2019). Microglia in retinal degeneration. Front. Immunol. *10*, 1975. https://doi.org/10.3389/fimmu.2019.01975.

Santos, A.M., Calvente, R., Tassi, M., Carrasco, M.C., Martin-Oliva, D., Marin-Teva, J.L., Navascues, J., and Cuadros, M.A. (2008). Embryonic and postnatal development of microglial cells in the mouse retina. J. Comp. Neurol. *506*, 224–239. https://doi.org/10.1002/cne.21538.

Sedgwick, J.D., Schwender, S., Imrich, H., Dorries, R., Butcher, G.W., and ter Meulen, V. (1991). Isolation and direct characterization of resident microglial cells from the normal and inflamed central nervous system. Proc. Natl. Acad. Sci. U S A *88*, 7438–7442. https://doi.org/10.1073/pnas.88.16.7438.

Shaham, O., Menuchin, Y., Farhy, C., and Ashery-Padan, R. (2012). Pax6: a multi-level regulator of ocular development. Prog. Retin. Eye Res. *31*, 351–376. https://doi.org/10.1016/j.preteyeres.2012.04.002.

Stein-Streilein, J. (2013). Mechanisms of immune privilege in the posterior eye. Int. Rev. Immunol. *32*, 42–56. https://doi.org/10.3109/08830185.2012.740535.

Suga, A., Sadamoto, K., Fujii, M., Mandai, M., and Takahashi, M. (2014). Proliferation potential of müller glia after retinal damage varies between mouse strains. PLoS One *9*, e94556. https://doi.org/10.1371/journal.pone.0094556.

Terzic, J., and Saraga-Babic, M. (1999). Expression pattern of PAX3 and PAX6 genes during human embryogenesis. Int. J. Dev. Biol. *43*, 501–508.

Tremblay, M.E., Stevens, B., Sierra, A., Wake, H., Bessis, A., and Nimmerjahn, A. (2011). The role of microglia in the healthy brain. J. Neurosci. *31*, 16064–16069. https://doi.org/10.1523/JNEUROSCI.4158-11.2011.

Yoh, K., and Prywes, R. (2015). Pathway regulation of p63, a director of epithelial cell fate. Front. Endocrinol. (Lausanne) *6*, 51. https://doi.org/10.3389/fendo.2015.00051.

Zhang, X., Huang, C.T., Chen, J., Pankratz, M.T., Xi, J., Li, J., Yang, Y., Lavaute, T.M., Li, X.J., Ayala, M., et al. (2010). Pax6 is a human neuroectoderm cell fate determinant. Cell Stem Cell *7*, 90–100. https://doi.org/10.1016/j.stem.2010.04.017.

Zhong, X., Gutierrez, C., Xue, T., Hampton, C., Vergara, M.N., Cao, L.H., Peters, A., Park, T.S., Zambidis, E.T., Meyer, J.S., et al. (2014). Generation of three-dimensional retinal tissue with functional photoreceptors from human iPSCs. Nat. Commun. *5*, 4047. https://doi.org/10.1038/ncomms5047.

Stem Cell Reports, Volume *17*

Supplemental Information

PAX6-positive microglia evolve locally in hiPSC-derived ocular organoids

Nobuhiko Shiraki, Kazuichi Maruyama, Ryuhei Hayashi, Akiko Oguchi, Yasuhiro Murakawa, Tomohiko Katayama, Toru Takigawa, Susumu Sakimoto, Andrew J. Quantock, Motokazu Tsujikawa, and Kohji Nishida

Supplemental Information

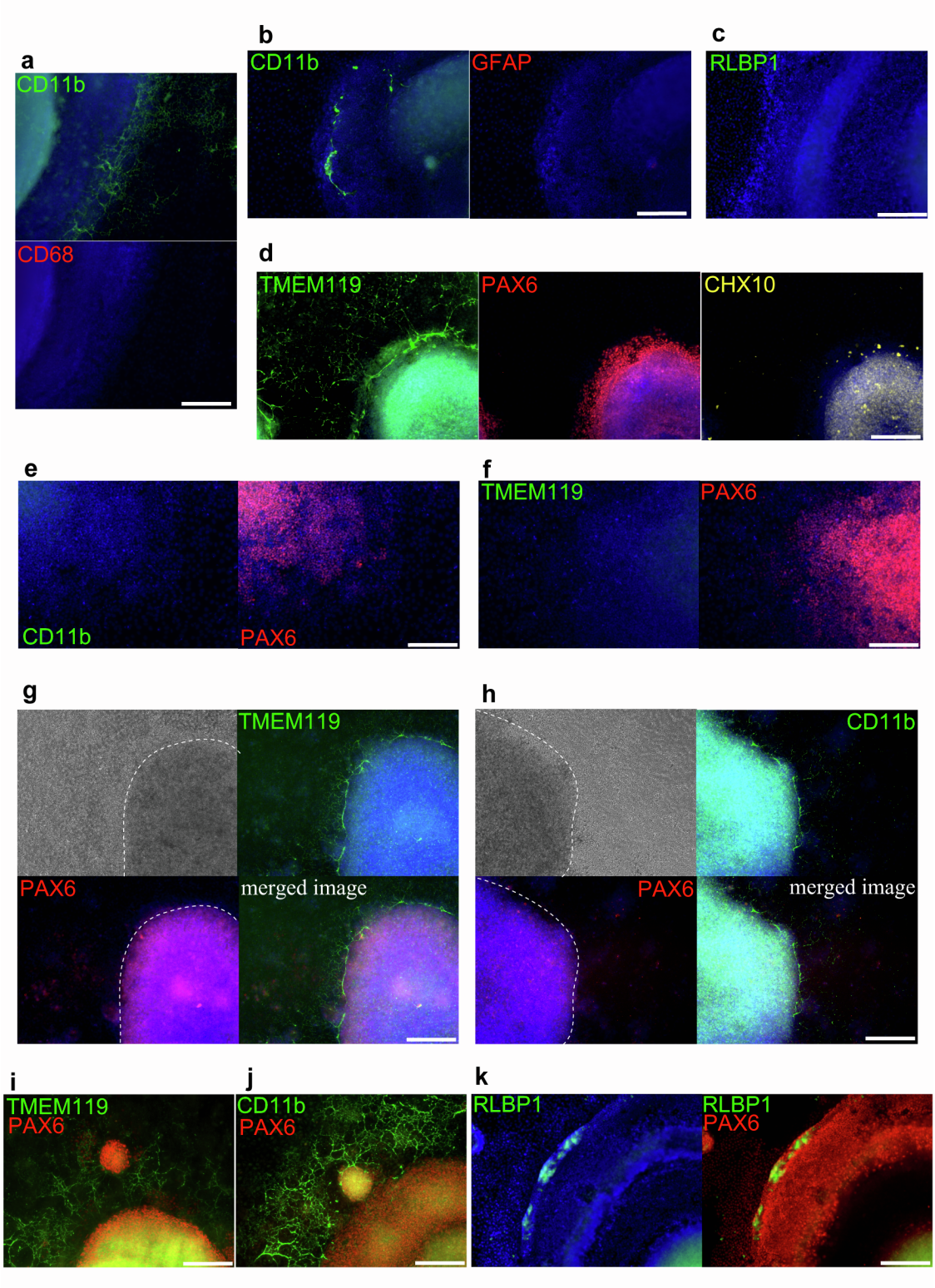

Figure S1. Immunostaining of 201B7 hiPSC-derived SEAMs. Related to figure 1.

Four-week differentiated SEAMs immunostained for (a) CD11b (green) and CD68 (red), (b) CD11b (green) and GFAP (red), (c) RLBP1(green), and (d) TMEM119 (green), PAX6 (red), and CHX10 (yellow). Also shown is an 8-day differentiated SEAM stained for (e) CD11b (green) and PAX6 (red) and (f) TMEM119 (green) and PAX6 (red), a 10-day differentiated SEAM stained for (g) TMEM119 (green) and PAX6 (red), and (h) CD11b (green) and PAX6 (red), and a 2-week differentiated SEAM stained for (i) TMEM119 (green) and PAX6 (red) and (j) CD11b (green) and PAX6 (red). (k) Immunostaining after 7-weeks of differentiation for retinal culture; RLBP1 Muller glia cells (green) and PAX6 (red). Images are representative of multiple independent experiments. Nuclei are in blue. Scale bar, 200 μm.

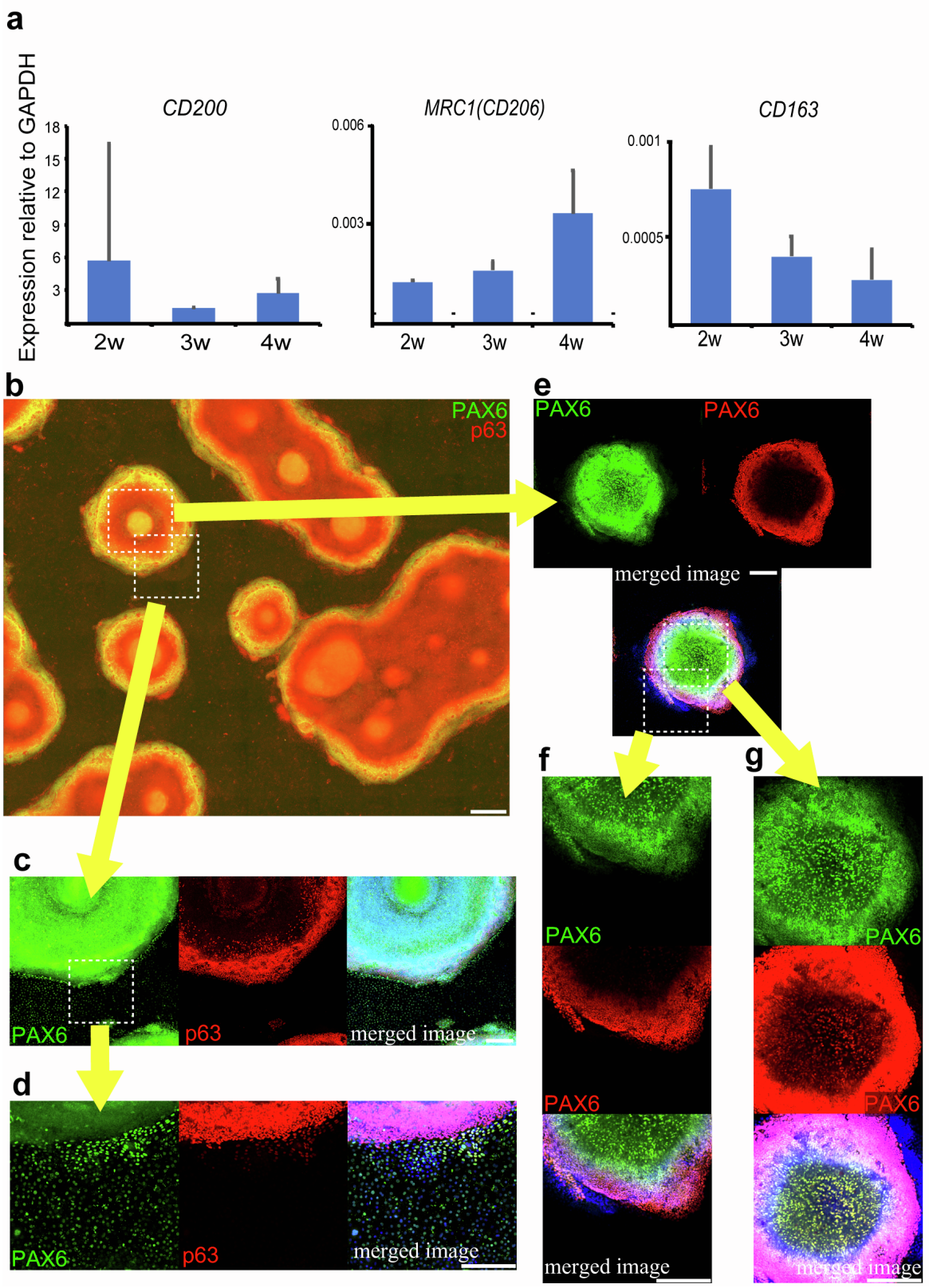

Figure S2. Expression of immune cell markers and immunostaining of

neuroectodermal and surface ectodermal markers. Related to figure 2.

a, Gene expression analysis of immune cell markers in a 201B7 hiPSC-derived SEAM at the 4-week culture point. Data are from six independent experiments. Error bars show SD. b-d, Immunostaining of PAX6 (green) in zone 1-3 and p63 (red) in zones 3-4 of a 4-week cultivated 201B7 hiPSC-derived SEAM. Images are representative of three independent experiments. Nuclei are in blue. Scale bar, 500 μm (b), 200um (c, d). e-g, Immunostaining for PAX6 (mouse monoclonal; green) and PAX6 (rabbit polyclonal; red) after proteolytic-induced epitope retrieval. It looks as if the center is not stained by PAX6 (rabbit polyclonal; red) because the around is too high brightness, both it is also stained by PAX6(green) and PAX6(red). Images are representative of three independent experiments. Nuclei are in blue. Scale bar, 200 μm.

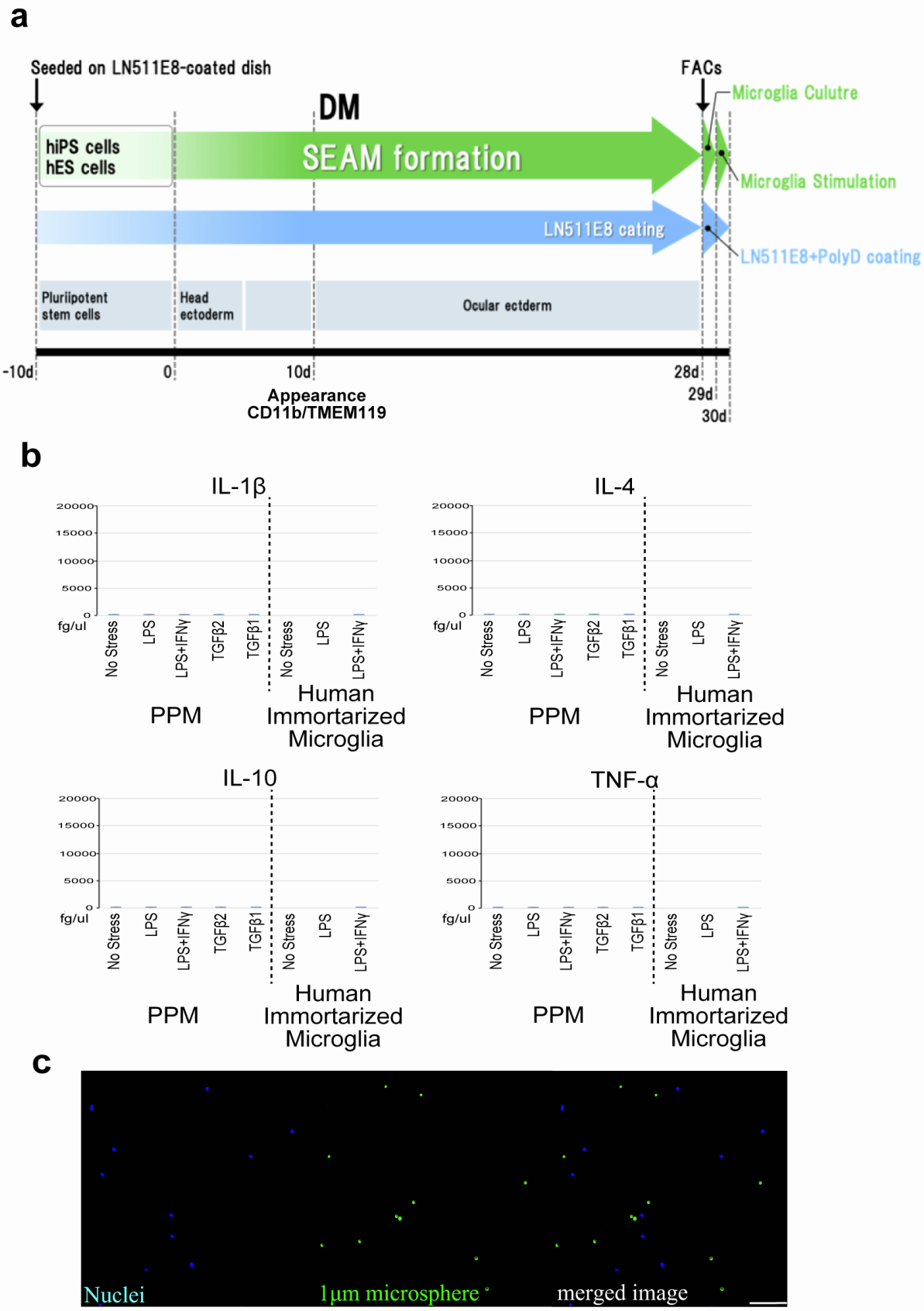
a
Seeded on LN511E8-coated dish
FACs
Microglia Culutre
DM
hiPS cells
hES cells
SEAM formation
Microglia Stimulation
LN511E8 cating
LN511E8+PolyD coating
Pluriipotent stem cells
Head ectoderm
Ocular ectderm
-10d
0
10d
28d
29d
30d
Appearance CD11b/TMEM119
b
IL-1β
IL-4
IL-10
TNF-α
20000
15000
10000
5000
0
fg/ul
No Stress
LPS
LPS+IFNγ
TGFβ2
TGFβ1
PPM
Human Immortarized Microglia
c
Nuclei
1μm microsphere
merged image

Figure S3. Schematic representation of the cultivation strategy, and quantification of cytokine secretion in SEAMs. Related to figure 3. a, Schematic representation of the strategy used for the generation of the ocular ectoderm and microglia. After 4 weeks of differentiation, the PPM cells were sorted and cultured for 24hours for cell recovery. And then they were stimulated for examination of the effect of inflammatory agents. DM, differentiation medium; w, week(s). b, Cytokine analysis for IL-1β, IL-4, IL-10, TNF-α after stimulation tests of PPM cells and human immortalised microglia cells. Data, respectively, are from two and six independent experiments. Error bars are s.d. c, Nuclei are in blue and 1μm microsphere are in green. CD11b+ cells were sorted by FACS and cytospin after four weeks of culture and were unable to phagocyte. Images represent three independent experiments. Scale bar, 100 μm.

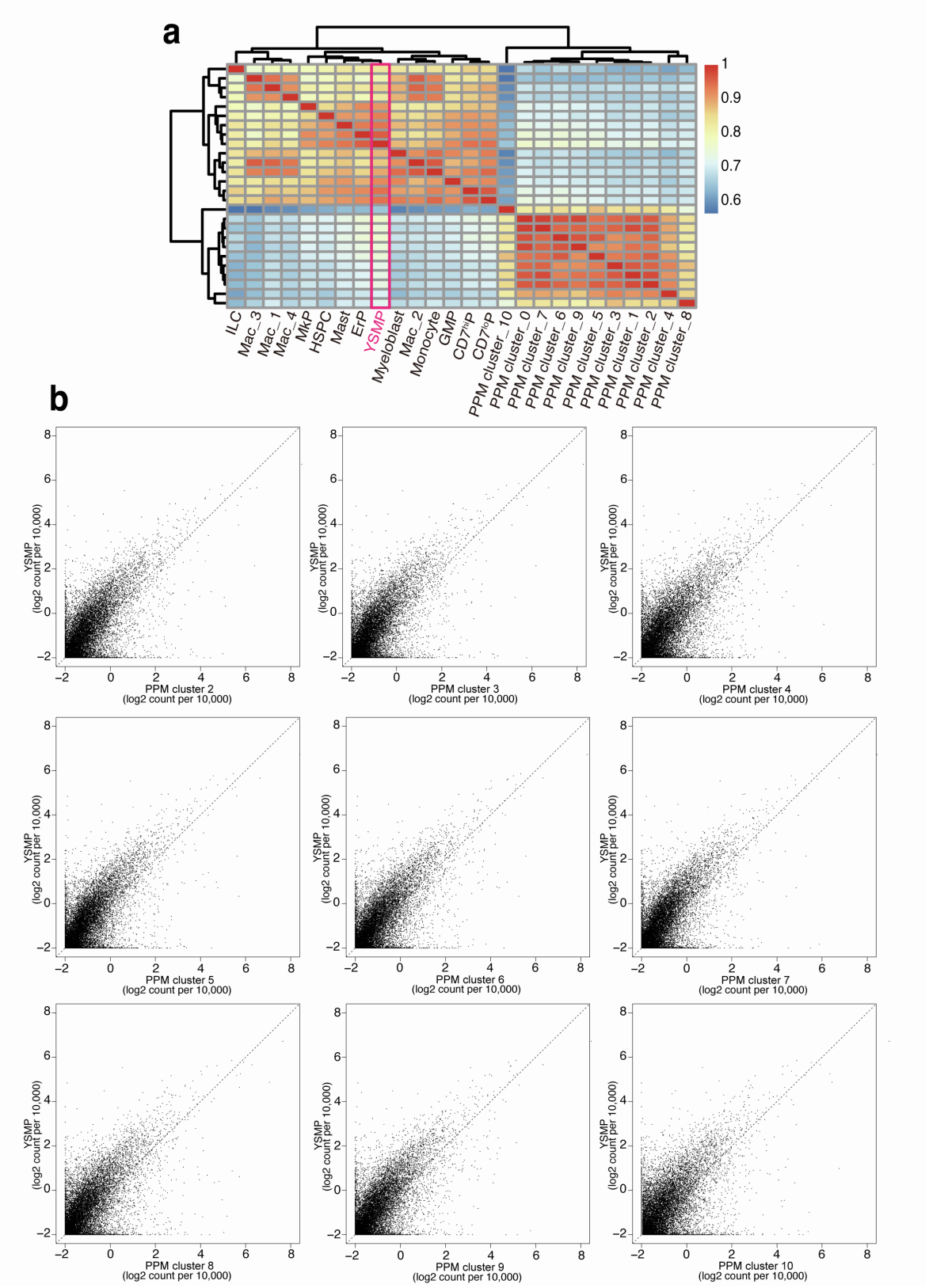

Figure S4. Single-cell RNA-seq analysis of SEAM-derived CD11b+ cells. Related to

figure 4.

(a) Heat map displaying a Pearson's correlation of gene expression for pairwise combinations among all cell clusters derived from CD11b+ cells and embryonic macrophages. (b) Scatterplots showing the gene expression of PPM cluster_2-9 identified in CD11b+ scRNA-seq along with that of the YSMP-cluster in scRNA-seq of embryonic macrophages.

Supplemental Video 1a, 1b. 3D structure of PPM cells (1a) and Enface movie of PPM cells (1b). Related to figure 1.

Immunostaining of TMEM119 (green) and PAX6 (red) in zones 1-3 of a 4-week cultivated SEAMs along with nuclei stained blue. (a) 3D movie (b) Enface movie (the direction is from top to bottom of the SEAM).

Supplemental Table 1 | a list of differential genes of each PPM clusters. Related to figure 4

Supplemental Table 2 | A list of the TaqMan probe sets. Related to figure 2 and 3

Target gene	Assay ID
GAPDH	Hs99999905_m1
SPI1	Hs02786711_m1
PAX6	Hs00240871_m1
SOX1	Hs01057642_m1
T	Hs00610080_m1
GATA4	Hs00171403_m1
SOX17	Hs00751752_s1
NKX2-5	Hs00231763_m1
SNAL1	Hs00195591_m1
TBX3	Hs00195612_m1
TGFβ2	Hs00234244_m1
VEGFA	Hs00900055_m1
ITGAM	Hs00167304_m1
CX3CR1	Hs01922583_s1
AIF1	Hs00610419_g1
CD56	Hs00941830_m1
MS4A1	Hs00254780_m1
CD68	Hs02836816_g1
MRC1	Hs07288635_g1
CD163	Hs00174705_m1
CD200	Hs01033302_m1
CD40	Hs01002915_g1

Supplemental Experimental Procedure

STAR★methods

KEY RESOURCES TABLE

REAGENT or RESOURCE	SOURCE	IDENTIFIER
Antibodies		
Rabbit polyclonal anti-CD11b	Abcam	Cat# ab133357, RRID:AB_2650514
Rabbit polyclonal anti-TMEM119	Sigma-Aldrich	Cat# HPA051870, RRID:AB_2681645
Mouse monoclonal anti-PAX6	Santa Cruz Biotechnology	Cat# sc-53108, RRID:AB_630089
Rabbit polyclonal anti-CD68	Abcam	Cat# ab31630, RRID:AB_1141557
Rabbit polyclonal anti-GFAP	Sigma-Aldrich	Cat# MAB3402, RRID:AB_94844
Rabbit polyclonal anti-CHX10	Santa Cruz Biotechnology	Cat# sc-21690, RRID:AB_2216006
Rabbit polyclonal anti-RLBP1	Proteintech	Cat# 15356-1-AP, RRID:AB_2178530
Rat monoclonal anti-CD11b-FITC conjugate	BioLegend	Cat# 101206, RRID:AB_312789
Rat monoclonal anti-IgG2b-FITC conjugate	BioLegend	Cat# 400605, RRID:AB_326549

Mouse monoclonal anti-CD45 phycoerythrin (PE)/cyanine7 conjugate	BioLegend	Cat# 304016, RRID:AB_314404
Mouse monoclonal anti-IgG1 phycoerythrin (PE)/cyanine7 conjugate	BioLegend	Cat# 400126, RRID:AB_326448
Mouse monoclonal anti-CD45 APC conjugate	BioLegend	Cat# 304037, RRID:AB_2562049
Mouse monoclonal anti-IgG1 APC conjugate	BioLegend	Cat# 400120, RRID:AB_288868
Donkey anti-mouse IgG Alexa Fluor 488 conjugate	Life Technologies	Cat# A-21202; RRID: AB_141607
Donkey anti-rabbit IgG Alexa Fluor 488 conjugate	Life Technologies	Cat# A-21206, RRID:AB_2535792
Donkey anti-mouse IgG Alexa Fluor 568 conjugate	Life Technologies	Cat# A-10037 RRID:AB_2534013
Donkey anti-rabbit IgG Alexa Fluor 594 conjugate	Life Technologies	Cat# A-21207, RRID:AB_141637
Donkey anti-goat IgG Alexa Fluor 647 conjugate	Life Technologies	Cat# A-21447, RRID:AB_141844
Chemicals, peptides, and recombinant proteins		
Glasgow modified Eagle's medium	Life Technologies	Cat# 11710035
Dulbecco's Modified Eagle Medium/Nutrient Mixture F-12	Life Technologies	Cat# 11320033
iMatrix-511 (LN511E8)	Nippi	Cat# 892012
FBS	Life Technologies	Cat# 12483-020
TrypLE™ Express Enzyme (1X), phenol red	Thermo Fisher Scientific	Cat# 12605010
KnockOut™ Serum Replacement	Life Technologies	Cat# 10828-028
Sodium pyruvate	Life Technologies	Cat# 11360-070
Non-essential amino acids	Life Technologies	Cat# 11140-050

l-glutamine	Thermo Fisher Scientific	Cat# 25030081
Penicillin-streptomycin solution	Life Technologies	Cat# 15140-122
Monothioglycerol	Wako	Cat# 195-15791
Y-27632	Wako	Cat# 034-24024
Recombinant human KGF	Wako	Cat# 112-00813
B27™ supplement	Life Technologies	Cat# 17504-044
Prigrow II media	Abm	Cat# TM002
1% penicillin-streptomycin solution	Abm	Cat# G255
Applied Cell Extracellular Matrix	Abm	Cat# G422
poly-D-lysine	Sigma-Aldrich	Cat# P6407
QIAzol Lysis Reagent	QIAGEN	Cat# 79306
4% paraformaldehyde phosphate buffer solution	Wako	Cat# 163-20145
Tris-buffered saline	TaKaRa Bio	Cat# T903
Normal donkey serum	Jackson ImmunoResearch	Cat# 017-000-121
proteinase K	MACHEREY-NAGEL	Cat# 740506
Triton™-X 100	Sigma-Aldrich	Cat# T8787
Hoechst 33342	Wako	Cat# 346-07951
StemPro™ Accumax™ Cell Dissociation Reagent	Life Technologies	Cat# A11105-01
cell staining buffer	BioLegend	Cat# 420201
GultaMAX	Life Technologies	Cat# 35050061
lipopolysaccharide	Sigma-Aldrich	Cat# L2654
IFN-γ	Wako	Cat# 093-05631
TGFβ2	R&D Systems	Cat# 102-B2-001
TGFβ1	Wako	Cat# 209-16544
Critical commercial assays		
SuperScript™ III First-Strand Synthesis System for qRT-PCR	Life Technologies	Cat# 18080051

TaqMan™ Fast Universal PCR Master Mix (2X)	Life Technologies	Cat# 4364103
human chemokine CBA kit and the human enhanced sensitivity set	BD Biosciences	Cat# 561521
human cytokines and chemokines IL-1β	BD Biosciences	Cat# 561509,
human cytokines and chemokines IL-4	BD Biosciences	Cat# 561510,
human cytokines and chemokines IL-6	BD Biosciences	Cat# 561512,
human cytokines and chemokines IL-8	BD Biosciences	Cat# 561513,
human cytokines and chemokines IL-10	BD Biosciences	Cat# 561514,
human cytokines and chemokines TNF-α	BD Biosciences	Cat# 561516
fluorescent latex beads of 1 μm diameter	Sigma-Aldrich	Cat# L1030
miRNeasy mini kit	Qiagen	Cat# 21700
SMART-Seq HT kit	TaKaRa Bio	Cat# Z4455N
Chromium Single Cell A Chip Kit	10X Genomics	Cat# 1000009
Chromium Single Cell 3' library and Gel Bead Kit v3	10X Genomics	Cat# PN-1000092
Nextera DNA library preparation kit	Illumina	Cat# FC-121-1030
Experimental models: Cell lines		
Human: iPS cell line 1383D2	Center for iPS Cell Research and Application	N/A
Human: iPS cell line 201B7	RIKEN Bio Resource Center	Cat# HPS0063; RRID: CVCL_A324
Human: ES cell line KhES-1	RIKEN Bio Resource Centre	Cat# HES0001;RRID:CVCL_B231
Human: Immortalised human microglia-SV40 cells	Applied Biological Materials Inc	Cat# T0251
Oligonucleotides		
TaqMan probes were listed in Table S2	Life Technologies	Cat# 4331182
Software and algorithms		

FV31S ver 2.3.2	Olympus	https://www.olympus-lifescience.com/en/support/downloads/
FACSDiva software	BD Biosciences	https://www.bdbiosciences.com/ja-jp/instruments/research-instruments/research-software/flow-cytometry-acquisition/facsdiva-software
FCAP Array™ Software v3.0	BD Biosciences	https://www.bdbiosciences.com/en-us/products/instruments/software-informatics/instrument-software/fcap-array-software-v3-0.652099
Illumina Casava 1.8.2 software	Illumina	https://bioweb.pasteur.fr/packages/pack@casava@1.8.2/
R package Seurat v3.2.1	(Stuart et al., 2019)	N/A
Photoshop CS6	Adobe Inc.	http://www.adobe.com/
Illustrator CS6	Adobe Inc.	http://www.adobe.com/

JMP pro version 14.1.0	SAS Institute Inc	RRID: SCR_014242; https://www.jmp.com/en_us/software/predictive-analytics-software.html

EXPERIMENTAL MODELS AND SUBJECT DETAILS

Cell lines

The hiPSC line 201B7 was obtained from the RIKEN Bio Resource Centre (Tsukuba, Japan) (Takahashi et al., 2007), with 1383D2 hiPSCs provided by the Centre for iPS Cell Research and Application, Kyoto University (Nakagawa et al., 2014). KhES ES-1 cells were sourced from the RIKEN Bio Resource Centre (Fujioka et al., 2004). All hiPSCs and hES cells were cultured in StemFit medium (Ajinomoto, Tokyo, Japan) on LN511E8-coated (0.5 μg/cm^2) dishes (Barrandon and Green, 1987; Miyazaki et al., 2012). All experiments using recombinant DNA were approved by the Recombinant DNA Committee of Osaka University and were performed according to our institutional guidelines.

Immortalised human microglia-SV40 cells were purchased from Applied Biological Materials Inc. These had been immortalised by serial passaging and transduction with recombinant lentiviruses carrying SV40 Large T antigen (Applied Biomedical Materials: abm, Richmond, QC, Canada). The cells were grown in Prigrow II media (abm) containing 10% foetal bovine serum (FBS) and 1% penicillin-streptomycin solution (abm) in T25 flasks coated with Applied Cell Extracellular Matrix (abm) and seeded at a density of 35,000-40,000 cells/cm^2. DMEM-F12 medium was supplemented with 10% FBS in T25 flasks coated with poly-D-lysine (1.3 μg/cm^2) (Sigma-Aldrich, MO,6USA). Cells were passaged at 80% confluence.

METHODS DETAILS

SEAM formation from hiPSCs

SEAMs were generated as described (Hayashi et al., 2017; Hayashi et al., 2016). The hiPS or hES cells were seeded on LN511E8-coated dishes at a density of 300–600 cells/cm^2, after which they were cultured in StemFit medium for 10 days. The culture medium was then changed to differentiation medium (DM; Glasgow modified Eagle's

medium (Life Technologies) supplemented with 10% knockout serum replacement (KSR; Life Technologies), 1 mM sodium pyruvate (Life Technologies), 0.1 mM non-essential amino acids (Life Technologies), 2 mM L-glutamine (Life Technologies), 1% penicillin-streptomycin solution (Life Technologies), and 55 μM monothioglycerol (Wako, Osaka, Japan) (Hayashi *et al.*, 2017). To achieve retinal differentiation, after four weeks of culture in DM, the medium was changed to Dulbecco's modified Eagle's medium (DMEM)/F12 (1:1) (Life Technologies) containing 2% B27 supplement (Life Technologies), 1% penicillin-streptomycin solution, 10 ng mL^{-1} KGF (Wako), and 10 μM Y-27632 (Wako) for three weeks. Phase-contrast microscopy was performed using an Axio observer Z1, D1 (Carl Zeiss, Jena, Germany).

Immunofluorescence staining

Formed SEAMs were fixed with 4% paraformaldehyde and washed three times with Tris-buffered saline (TBS, TaKaRa Bio) for 10 min each. When they were stained simultaneously by PAX6 (AD2.35; Santa Cruz Biotechnology, Santa Cruz, CA, USA) and PAX6(901301, BioLegend, CA, USA), they were incubated with TBS containing

0.05% proteinase K for 5 min for proteolytic-induced epitope retrieval. They were then incubated with TBS containing 5% donkey serum and 0.3% Triton X-100 for 1 h to block non-specific binding followed by incubation overnight at 4 °C with primary antibodies against CD11b (ab133357; Abcam, Cambridge, UK), TMEM119 (HPA051870; Sigma-Aldrich), CX3CR1 (14-6093-81; Invitrogen), PAX6, CD68 (ab31630; Abcam), GFAP (MAB3402; Sigma-Aldrich), CHX10 (sc-21690; Santa Cruz), and RLBP1(15356-1-AP; proteintech). The SEAMs were again washed three times with TBS for 10 min, and incubated with 1:200 dilution of Alexa Fluor 488-, 568-, and 647-conjugated secondary antibodies (Life Technologies) for 1 h at room temperature. Counterstaining was performed with Hoechst 33342 (Life Technologies). Images were captured using fluorescence microscopy (Axio Observer.D1, Carl Zeiss) or confocal microscopy (FV3000, Olympus, Tokyo, Japan) and processed using AxioVision ver 4.8.1 (Carl Zeiss), FV31S ver 2.3.2 (Olympus) and Adobe Photoshop 2020 (Adobe Inc., San Jose, CA, USA).

Flow cytometry and cell sorting

SEAMs cultured in DM for 4-weeks were dissociated using Accumax (Life Technologies) for 10 min at 37 °C and resuspended in ice-cold cell staining buffer (420201, BioLegend, CA, USA), after which the harvested cells were filtered using a cell strainer. They were stained with CD11b-FITC antibody (101206, BioLegend), FITC rat IgG2b (400605, BioLegend), phycoerythrin (PE)/cyanine7 anti-human CD45 (304016, BioLegend), PE/Cy7 mouse IgG1 (400126, BioLegend), APC anti-human CD45 antibody (304037, BioLegend), and APC mouse IgG1 (400120, BioLegend) for 30 min on ice (Ford et al., 1995; Sedgwick et al., 1991). After washing three times with PBS, the stained cells were sorted using a FACSAria II instrument (BD Biosciences), and the data were analysed using BD FACSDiva software (BD Biosciences). CD11b positive cells, which did not express high levels of CD45, were harvested. After sorting, some of the cells were used for cytospin, while the remaining cells (now with the identity of PPM cells) were seeded on poly-D-lysine-coated (1.3 μg/cm^2) and LN511E8-coated (0.5 μg/cm^2) dishes at the density of 1.6–2.4 × 10^5 cells/cm^2 and cultured in microglial culture medium (MCM; DMEM/F12 (1:1) supplemented with 10% FBS (Japan Bio Serum, Hiroshima, Japan), 1% GultaMAX (Thermo Fisher

Scientific), and 1% penicillin-streptomycin solution). The sorted PPM cells were adjusted to a density of 2×10^5 cells/mL, after which 200 µL of the cell suspension was centrifuged at 1000 rpm for 5 min in a CytospinTM 4 Cytocentrifuge (Thermo Fisher Scientific).

Cell stimulation

To examine the effect of inflammatory agents, PPM cells and immortalized microglia cells were cultured for 24 h and further stimulated for 24 h with lipopolysaccharide (LPS; 1 µg/mL) (Sigma-Aldrich), LPS (1 µg/mL) and IFN-γ (200 ng/mL) (Wako), TGF-β2 (5 ng/mL) (R&D Systems, MN, USA), or TGF-β1 (5 ng/mL) (Wako) added to the culture media. The medium was then collected in protein low-adhesion tubes, and the cells were stored in QIAzol reagent (Qiagen, Valencia, CA, USA).

qRT-PCR

Total RNA was obtained using QIAzol from cells in SEAMs at 1-week and 4-weeks of differentiation, and from PPM cells and immortalised human microglia cells with and

without stimulation. Reverse transcription was performed using the SuperScript III first-strand synthesis system for qRT-PCR (Life Technologies) according to the manufacturer's protocol, and the cDNA was used as a template for PCR. qRT-PCR was performed on the ABI Prism 7500 Fast Sequence Detection system (Life Technologies) according to the manufacturer's instructions. The TaqMan MGB used in this study is shown in Table S1. The thermocycling was performed with an initial cycle at 95°C for 20s, followed by 45 cycles at 95°C for 3s and 60°C for 30 s

Cytokine analysis

Cell culture supernatant samples were collected 24 h after stimulating the PPM cells and human immortalised microglia cells. Commercial kits for the detection of human cytokines and chemokines (IL-1β, IL-4, IL-6, IL-8, IL-10, and TNF-α) (561509, 561510, 561512, 561513, 561514, and 561516; BD Biosciences) were screened for cross-reactive detection of homologous macaque proteins. Levels of each factor were assayed using the human chemokine CBA kit and the human enhanced sensitivity set (561521; BD Biosciences) according to the manufacturer's instructions. The samples

were acquired with the FACS Verse instrument (BD Biosciences) and the data were analysed using CBA and FCAP software (BD Biosciences).

Phagocytosis Assay

Phagocytosis Assay was performed using 1 μm polystyrene FluoSpheres (Sigma-Aldrich). After 24 h culture for the recovery of microglial cells, PPM cells were tested by the phagocytosis assay. The aqueous green fluorescent latex beads in FBS for 1 h at 37 °C were pre-opsonized. The ratio of beads to FBS was 1:5. The bead-containing FBS was diluted with MCM to reach the final concentrations for beads and FBS in MCM of 0.01% and 0.05%, respectively. The microglial conditioned culture media were replaced with beads containing MCM, and the cultures were incubated at 37 °C for 1 h. The cultures were washed thoroughly with ice-cold PBS 5 times; thereafter, the cells were fixed using 4% PFA for 15 min (Lian et al., 2016).

RNA-seq

Samples were obtained from the cells sorted by FACS and cultured for 24 h with a

stimulating medium for the microglia. Total RNA was extracted from the cells using a miRNeasy mini kit (Qiagen) according to the manufacturer's protocol. Full-length cDNA was generated using a SMART-Seq HT kit (TaKaRa Bio, Mountain View, CA, USA) according to the manufacturer's instructions. The sequencing library was prepared using a Nextera DNA library preparation kit (Illumina, San Diego, CA, USA) according to SMARTer kit instructions. Sequencing was performed on an Illumina NovaSeq 6000 sequencer (Illumina) in the 100-base single-end mode. Illumina Casava 1.8.2 software was used for base calling. The sequenced reads (30M reads, single-end 100 bp) were mapped to the human reference genome sequence (hg19) using TopHat v2.0.12. Fragments per kilobase of exons per million mapped fragments (FPKMs) were calculated using Cufflinks v 2.1.1.

Single-cell library preparation and sequencing

CD11b+ cells were isolated using the same protocol as described in the DMEM/F12 with 10% FBS section. Cell suspension was loaded to a Chromium Single Cell Chip (10x Genomics) according to the manufacturer's instructions. Sample was processed

using the Chromium Single Cell 3’ library and Gel Bead Kit v3 (10X Genomics) following the manufacturer’s instructions. Single-cell library was sequenced with an 8-base index read (Chromium i7Sample Index (PN-220103, SI-GA-E3)), a 5’-CTACACGACGCTCTTCCGATCT-3’-base read1(PN-2000089), and a 5’-GATCGGAAGAGCACACGTCTGAACTCCAGTCA-3’-base read 2(PN -2000094) on an Illumina HiSeq X platform.

Single-cell data processing

FASTQ files were processed using the “cellranger count” pipeline from Cell Ranger version 3.0.2 (10× Genomics) with GRCh38 v.3.0.0 Cell Ranger reference. The subsequent data analysis was performed using R package Seurat v3.2.1. We followed the Seurat vignette (https://satijalab.org/seurat/pbmc3k_tutorial.html) to create the Seurat data matrix object. In brief, we kept all genes expressed in more than three cells and cells with at least 200 detected genes. Cells with mitochondrial gene percentages >25% and unique gene counts <1000 were discarded. The data were normalized using Seurat’s “NormalizeData” function, in which UMI counts for each gene from each cell

were divided by the total UMI counts from that cell, multiplied by the scale factor of 10,000 and natural log-transformed. Highly variable genes were then identified using the function “FindVariableGenes” in Seurat with default parameters. We regressed out the variation arising from the library size and percentage of mitochondrial genes using the function “ScaleData” in Seurat. Principal component analysis (PCA) for dimensionality reduction was performed using the Seurat “RunPCA” function. The computed PCs were used to perform unsupervised cell clustering using the functions “FindClusters” and to make UMAP results of scRNA-Seq data using the Seurat “RunUMAP” function. The number of PCs used in each analysis is noted in the Figure legends. To identify differentially expressed genes in each cell cluster, we used the function “FindAllMarkers” in Seurat on the normalized gene expression data.

Comparison with scRNA-seq data of embryonic macrophages

Publicly available scRNA-seq data of embryonic macrophages were downloaded from the Gene Expression Omnibus (GEO) under accession GSE133345. To calculate the average gene expression within clusters which the authors annotated, the sum of UMI

counts for each gene from each cluster was divided by the total UMI counts from that cluster, multiplied by the scale factor of 10,000 and log(2)-transformed. A prior count of 0.25 was added before log-transformation. The average gene expression within each cluster from our CD11b+ scRNA-data was acquired using the Seurat "AverageExpression" function with option "return.seurat = F". The average gene expression was log(2)-transformed, with a prior count of 0.25 added before log-transformation.

Quantification and statistical analysis

All statistical analyses were conducted with JMP Pro version 14.1.0. Data are presented as standard errors of the means (SEMs); n represents biological repeats. Statistical analyses were performed by Mann-Whitney U tests for comparisons of two groups and by Steel's tests for multiple comparisons. Differences with *P*-values of less than 0.05 were considered statistically significant. Further details are provided in the context of each specific assay in the relevant section of the Figure legends.

Supplemental resource availability

Lead contact

Further information and requests for resources and reagents should be directed to the Lead Contact, Kazuichi Maruyama (kazuichi.maruyama@ophthal.med.osaka-u.ac.jp) or Kohji Nishida (knishida@ophthal.med.osaka-u.ac.jp).

Materials availability

Unique materials generated in this study are available from the Lead Contact upon reasonable request following the signing of a Materials Transfer Agreement.

Data and code availability

All data are available in the main Article or the Supplementary Information and from the corresponding author upon reasonable request. Source data are provided with this paper. Raw data from RNA-seq and scRNA-seq analysis have been deposited in the NCBI Gene Expression Omnibus (GEO) under accession number GSE190429.

Supplemental Refferences

Barrandon, Y., and Green, H. (1987). Three clonal types of keratinocyte with different capacities for multiplication. Proc Natl Acad Sci U S A *84*, 2302-2306. 10.1073/pnas.84.8.2302.

Ford, A.L., Goodsall, A.L., Hickey, W.F., and Sedgwick, J.D. (1995). Normal adult ramified microglia separated from other central nervous system macrophages by flow cytometric sorting. Phenotypic differences defined and direct ex vivo antigen presentation to myelin basic protein-reactive CD4+ T cells compared. J Immunol *154*, 4309-4321.

Fujioka, T., Yasuchika, K., Nakamura, Y., Nakatsuji, N., and Suemori, H. (2004). A simple and efficient cryopreservation method for primate embryonic stem cells. Int J Dev Biol *48*, 1149-1154. 10.1387/ijdb.041852tf.

Hayashi, R., Ishikawa, Y., Katori, R., Sasamoto, Y., Taniwaki, Y., Takayanagi, H., Tsujikawa, M., Sekiguchi, K., Quantock, A.J., and Nishida, K. (2017). Coordinated generation of multiple ocular-like cell lineages and fabrication of functional corneal epithelial cell sheets from human iPS cells. Nat Protoc *12*, 683-696. 10.1038/nprot.2017.007.

Hayashi, R., Ishikawa, Y., Sasamoto, Y., Katori, R., Nomura, N., Ichikawa, T., Araki, S., Soma, T., Kawasaki, S., Sekiguchi, K., et al. (2016). Co-ordinated ocular development from human iPS cells and recovery of corneal function. Nature *531*, 376-380. 10.1038/nature17000.

Lian, H., Roy, E., and Zheng, H. (2016). Microglial Phagocytosis Assay. Bio Protoc *6*. 10.21769/BioProtoc.1988.

Miyazaki, T., Futaki, S., Suemori, H., Taniguchi, Y., Yamada, M., Kawasaki, M., Hayashi, M., Kumagai, H., Nakatsuji, N., Sekiguchi, K., and Kawase, E. (2012). Laminin E8 fragments support efficient adhesion and expansion of dissociated human pluripotent stem cells. Nat Commun *3*, 1236. 10.1038/ncomms2231.

Nakagawa, M., Taniguchi, Y., Senda, S., Takizawa, N., Ichisaka, T., Asano, K., Morizane, A., Doi, D., Takahashi, J., Nishizawa, M., et al. (2014). A novel efficient feeder-free culture system for the derivation of human induced pluripotent stem cells. Sci Rep *4*, 3594. 10.1038/srep03594.

Sedgwick, J.D., Schwender, S., Imrich, H., Dorries, R., Butcher, G.W., and ter Meulen, V. (1991). Isolation and direct characterization of resident microglial cells from the normal and inflamed central nervous system. Proc Natl Acad Sci U S A *88*, 7438-7442. 10.1073/pnas.88.16.7438.

Takahashi, K., Tanabe, K., Ohnuki, M., Narita, M., Ichisaka, T., Tomoda, K., and Yamanaka, S. (2007). Induction of pluripotent stem cells from adult human fibroblasts by defined factors. Cell *131*, 861-872. 10.1016/j.cell.2007.11.019.